Available online at www.sciencedirect.com
SCIENCE DIRECT
Journal of Power Sources 158 (2006) 754–759
JOURNAL OF POWER SOURCES
www.elsevier.com/locate/jpowsour

Short communication

Recycling of nickel from NiOOH/Ni(OH)$_2$ electrodes of spent Ni–Cd batteries

A. Rozário, R.K. Silva e Silva, M.B.J.G. Freitas *

Universidade Federal do Espírito Santo, Departamento de Química, Laboratório de Eletroquímica Aplicada, Av. Fernando Ferrari s/n, Goiabeiras, Vitória-ES, CEP 29060-900, Brazil

Received 18 July 2005; accepted 10 August 2005
Available online 16 November 2005

Abstract

In this work, nickel from the positive electrode of Ni–Cd batteries was recycled by chemical precipitation and electrodeposition. The structure of the material recovered by chemical precipitation is affected by temperature. Alfa nickel hydroxide is stable at low temperature but becomes beta nickel hydroxide with increasing of the synthesis temperature. Electrodeposition was accomplished by using the galvanostatic technique. The chronopotentiometric plots presented a plateau potential in the initial stage of the deposit growth due to the reduction of ionic nickel. Charge density of the plateau potential and charge efficiency decreased with increase in current density. Charge efficiency around 81.0% was the largest for current densities between 5.0 mA cm^{-2} and 10.0 mA cm^{-2} for $q = 9.0$ C cm^{-2}. As charge density increased to 90.0 C m^{-2}, the electrodeposition efficiency decreased. In this case, there is a second plateau potential at which the evolution of hydrogen on the nickel electrode, the principal reaction, is quickly reached. Charge density affects not only the reaction kinetics, but also the deposit morphology. A decrease in microporosity is observed with the increase in charge density. The microporosity increases as the current density increases for the same charge density.
© 2005 Elsevier B.V. All rights reserved.

Keywords: Nickel; Recycling; Ni–Cd battery

1. Introduction

Ni–Cd batteries have been used since 1950 in applications that require high energy density, long life, and high discharge ratios. Ni-MH and lithium batteries also have these characteristics, but they are costlier. For this reason, Ni–Cd batteries are still largely used in many parts of the world [1–3]. The positive electrode of Ni–Cd batteries is made up of NiOH/Ni(OH)$_2$ and additives such as graphite and cobalt, and the negative electrode is made of cadmium. The positive and negative electrodes are isolated by polyethylene, cardboard, or polypropylenes separators. The electrolyte is a solution made of KOH and LiOH. The general discharge reaction of the Ni–Cd battery is:

$$2\mathrm{NiOOH} + \mathrm{Cd} + 2\mathrm{H_2O} \rightarrow 2\mathrm{Ni(OH)_2} + \mathrm{Cd(OH)_2} \quad (1)$$

The precursor material used in positive electrodes, Ni(OH)$_2$, can be found in phases α-Ni(OH)$_2$ or β-Ni(OH)$_2$. α-Ni(OH)$_2$ has a layered structure. In this structural arrangement, water and cation molecules are interspersed between layers. The distance between planes [0 0 1] is 8.05 Å. α-Ni(OH)$_2$ is unstable in the presence of an alkali and becomes β-Ni(OH)$_2$ as a result of aging, i.e., the elimination of water, cations, and consequently the contraction of the interplanar spaces. β-Ni(OH)$_2$ has a hexagonal structure with interplanar distance between planes [0 0 1] equal to 4.65 Å. β-Ni(OH)$_2$ is still largely used as a precursor material of positive electrodes of alkaline batteries [4–7]. However, α-Ni(OH)$_2$ has shown to be a promising material, mainly because it does not provoke electrode volume expansion during charge–discharge cycles. Expansion followed by volume contractions eventually lead to cracks, which prevent electric contact between the electrode regions. A consequence of this fact is the reduction of the capacity and the useful life of the positive electrodes [8,9]. The active material, NiOOH, can have either the β-NiOOH or the γ-NiOOH structure.

The Ni–Cd batteries are classified as a hazardous residue and spent Ni–Cd batteries should not be thrown to domestic garbage or sanitary landfills [10,11]. They must be collected by the manufacturers for recycling. The industry recycles Ni–Cd batteries

* Corresponding author. Tel.: +55 2733352486; fax: +55 2733352460.
E-mail address: marcosbj@hotmail.com (M.B.J.G. Freitas).

0378-7753/$ – see front matter © 2005 Elsevier B.V. All rights reserved.
doi:10.1016/j.jpowsour.2005.08.055

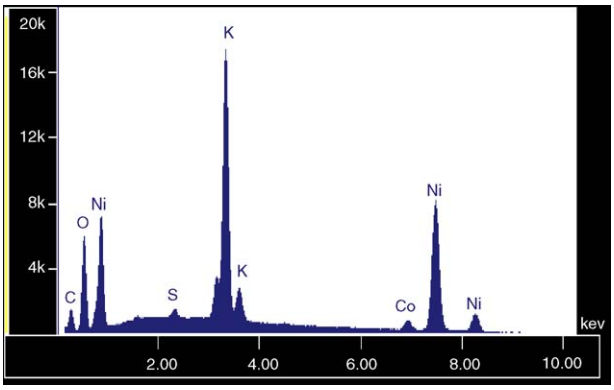

Fig. 1. Typical energy dispersive of X-ray of the positive electrode from the spent Ni–Cd batteries.

either by pyrometallurgic or hydrometallurgic process [12]. The pyrometallurgic process is not appropriate due to the emission of toxic gases in the environment. The hydrometallurgic process is more appropriate from the environment conservation viewpoint. This process consists of associated chemical and electrochemical transformations. Electrochemical recycling is also viable as it does not produce toxic substances and it also has academic interest [13,14]. In this work, nickel was recovered by chemical precipitation with the addition of NaOH 1.0 mol l^{-1} to the leaching solution at different temperatures. Nickel also was recovered by electrodeposition. The relation between current density, charge efficiency, and deposit morphology was analyzed. Ionic nickel was deposited onto 1020 steel from a leaching solution by a galvanostatic technique. The materials were characterized by the following techniques: X-ray diffraction, scanning electronic microscopy (SEM), X-ray energy-dispersive spectrometry (EDX), conductometry, and pHmetry.

2. Experimental

Battery recycling requires selective collection and disassembly of batteries and a sequence of physical and electrochemical transformations. Spent type-AA Ni–Cd batteries produced by Toshiba (3.6 V, 600 mAh) was used in this research. In the selective collection, spent batteries were classified in homogeneous lots. In the disassembly, spent batteries were physically separated into their different parts: anode, cathode, steel, separators, and current collectors. On average, the total weights of Ni–Cd battery parts corresponded to: anode 29% (w/w), cathode 32% (w/w), and steel, separators and current collectors 39% (w/w).

Cathode dissolution was accomplished with a solution of H_2SO_4 0.5000 mol l^{-1}. The mass of the positive electrode used was equal to 4.977 g, to which 496.0 ml of a solution of H_2SO_4 0.5000 mol l^{-1} was added. After 3.0 h, the dissolution of the electrode material occurs. The substratum was dried, resulting in a mass of 0.6485 g.

The precursor material was obtained by chemical precipitation at 279 K and 295 K. A solution of NaOH 1.000 mol l^{-1} was added to the leaching solution by dripping. Conductivity and pH were measured with each addition of 1.0 ml of NaOH 1.000 mol l^{-1} solution. It can be observed that initially the pH increased and the conductivity decreases gradually and slightly

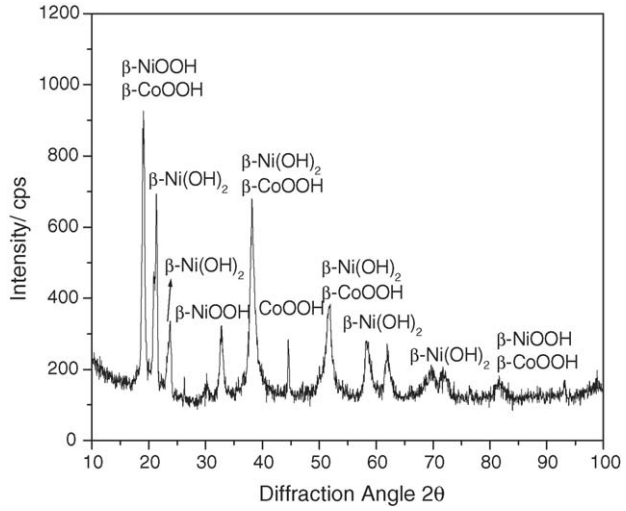

Fig. 2. Typical X-ray diffraction of the positive electrode from the spent Ni–Cd batteries.

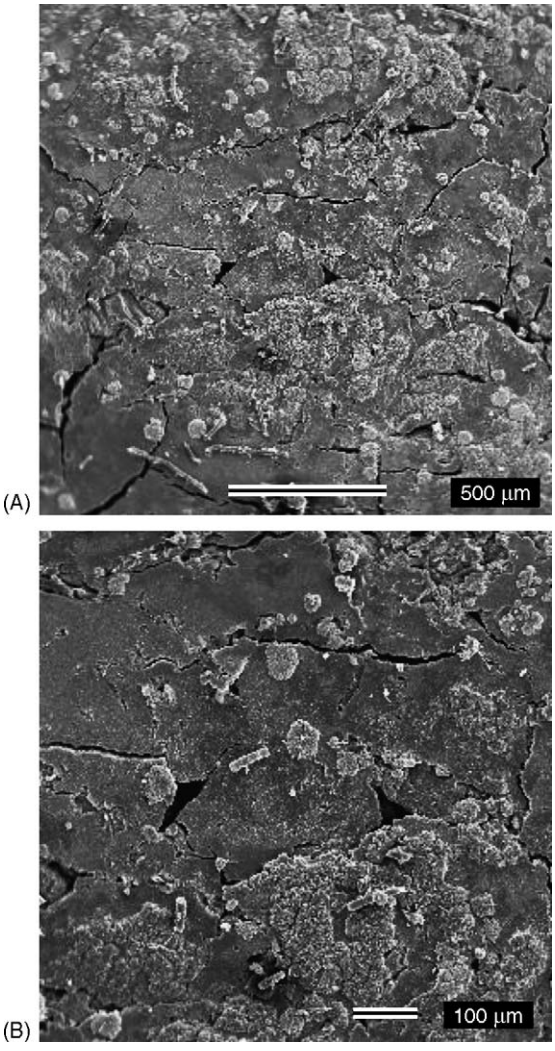

Fig. 3. Typical scanning electron microscopy (SEM) of the positive electrode from the spent Ni–Cd batteries: (A) 50× and (B) 100×.

due to the increasing neutralization of H^+ ions. The pH and the conductivity remained constant because of the formation of precipitate. Next, pH and the conductivity increased again due to excess of OH^- ions in the solution. The precipitate was filtered and washed with distilled water to remove excess reagent. $BaCl_2$ 1.000 mol l^{-1} was added to an aliquot of the wash water until there was no further $BaSO_4$ precipitation.

The working electrode was made of 1020 steel. The part of the electrode where there was to be no deposition was isolated with resin. The active area obtained was 0.2 cm^2. The auxiliary electrode was platinum with a geometric area of 3.75 cm^2. The reference electrode was Ag/AgCl/NaCl saturated. Before each electrochemical experiment, the working electrodes were sanded with 600 grit sandpaper and then rinsed with distilled water. Galvanostatic experiments were carried out with a laboratory-built regulated power supply. The charge density used was 9.0 C cm^{-2} and 90.0 C cm^{-2} and the current density varied between 5.0 mA cm^{-2} and 50.0 mA cm^{-2}.

The working and auxiliary electrodes were connected to a voltmeter and to a microcomputer by an RS232 interface. The electrolyte solutions were prepared with reagent p.a. and pure water. Solutions were changed after each experiment. All electrochemical experiments were performed at 298 K.

3. Results and discussions

3.1. Characterization of positive electrodes

Fig. 1 shows the constituent elements of the cathode surface. The largest peak observed corresponds to potassium from potassium hydroxide solution used as an electrolyte in alkaline batteries. The cobalt peak is from the use of cobalt hydroxide as an additive in this type of electrode to improve its efficiency. The sulphur detected is from carbon used to coat the samples and oxygen may either come from the electrolyte or NiOOH/$Ni(OH)_2$.

Fig. 2 presents a typical diffractogram of NiOOH/$Ni(OH)_2$ electrodes. In comparison with JCPDS cards [15–17], a not totally discharged positive electrode contains mostly phase β-$Ni(OH)_2$ and β-NiOOH. The diffraction peaks enlargement were due to small crystallite size and the overposition peaks of β-$Ni(OH)_2$, β-CoOOH, and β-NiOOH. The cracks due to the molar volume variation in charge–discharge cycles can be seen in the micrographs (SEM) in Fig. 3. The cracks limit discharge and reduce the useful life of the positive electrodes.

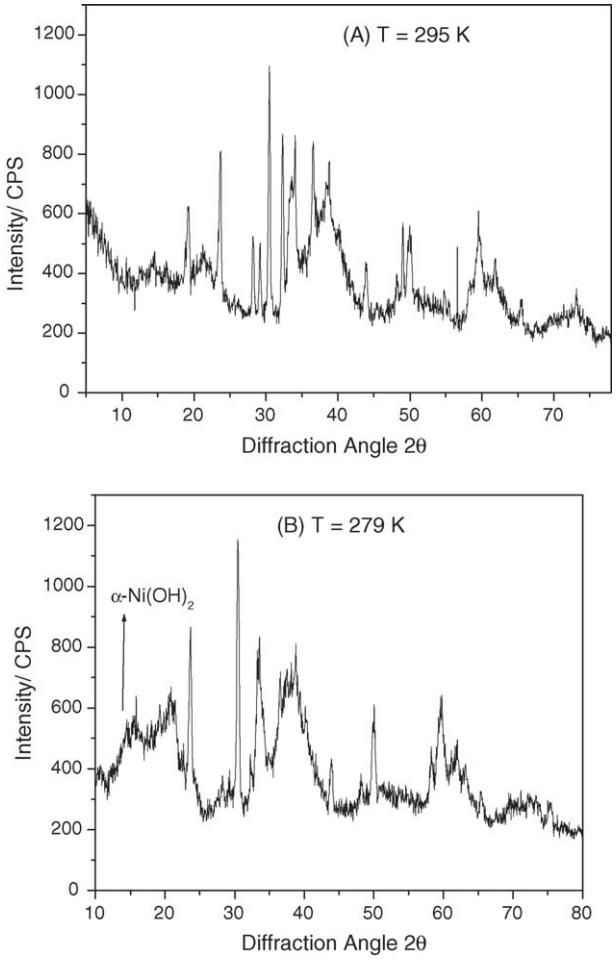

Fig. 4. Typical X-ray diffraction of the synthesized material: (A) 295 K and (B) 279 K.

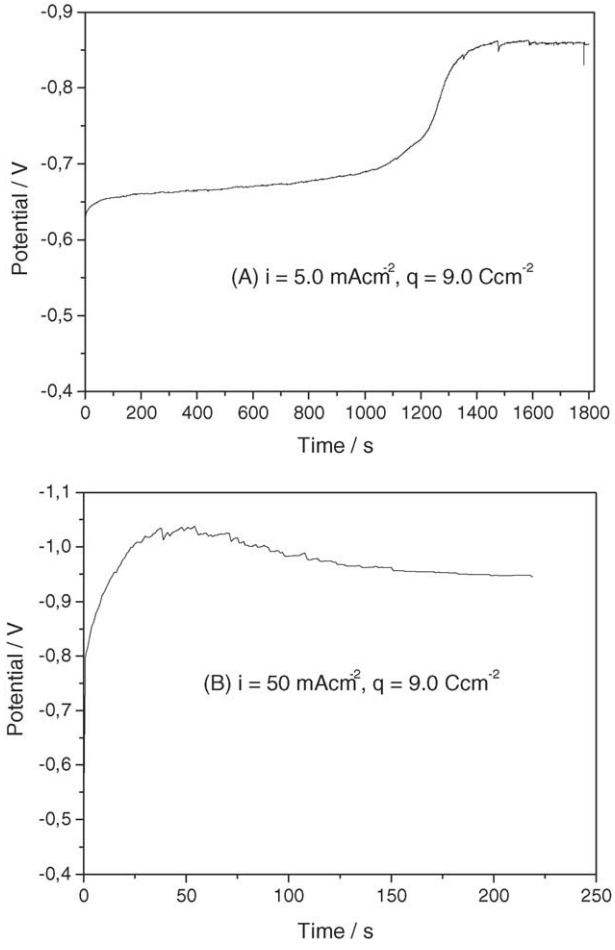

Fig. 5. Typical chronopotentiometric plot for nickel electrodeposition from leaching solution, without stirring: (A) i = 5.0 mA cm^{-2} and (B) i = 50 mA cm^{-2}, $q_{applied}$ = 9.0 C cm^{-2}, 298 K.

3.2. Characterization of the precursor material

Fig. 4 shows typical diffractograms of the precursor material synthesized at 295 K and 279 K. According to the JCPDS cards, the material synthesized at 295 K corresponds to phase β-$Ni(OH)_2$ and β-$Co(OH)_2$ [18]. However, in the diffractograms for materials synthesized at 279 K (Fig. 4B) observed a peak at 15°. This happens because water molecules and alkali metal ions intercalated in the plane [0 0 1] increase the interlayer distance and provoke a decrease in the diffraction angle as observed in Fig. 4B. The peak at 15° corresponds to phase α-$Ni(OH)_2$. The other peaks in that diffractogram just change the relative intensity. The presence of these two phases in the precursor material has great importance. A mixture of α-$Ni(OH)_2$ and β-$Ni(OH)_2$ rather than only β-$Ni(OH)_2$ increases the capacity of the positive electrode [8].

3.3. Electrochemical recycling

Nickel was recycled from an acidic solution with different charge densities by a galvanostatic technique. With the change in charge density, it was possible to analyze the different stages of the formation of the deposit. As shown in Fig. 5, the reaction potential stabilized on the first plateau of the chronopotentiometric plot for a constant charge density of 9.0 C cm^{-2} and a current density equal to 5.0 mA cm^{-2}. The charge density of the first plateau potential decreased with the increase in the current density. Either the reduction reaction of ionic nickel or the evolution of hydrogen owned on the nickel substrate when the electrode surface was covered with at least a monolayer of nickel. This occurred as the deposition time increased. With the increase in electrodeposition time, the potential became more cathodic and stabilized on a second plateau. At this second plateau potential, the evolution of hydrogen on the nickel electrode was the principal reaction. In the chronopotentiometric plot shown in Fig. 6 for a charge density of 90.0 C cm^{-2} and a current density equal to 5.0 mA cm^{-2}, we observed as low increase in the cathodic potential until a charge density of 30.0 C cm^{-2} ($t = 6000$ s) was reached. The evolution of hydrogen was the principal reaction after this point and a fast potential change was observed. For current densities over 5.0 mA cm^{-2}, a transient potential in the chronopotentiometric plots was observed as soon the current was applied. This transient potential was associated with the evolution of hydrogen and the formation of active sites by nucleation.

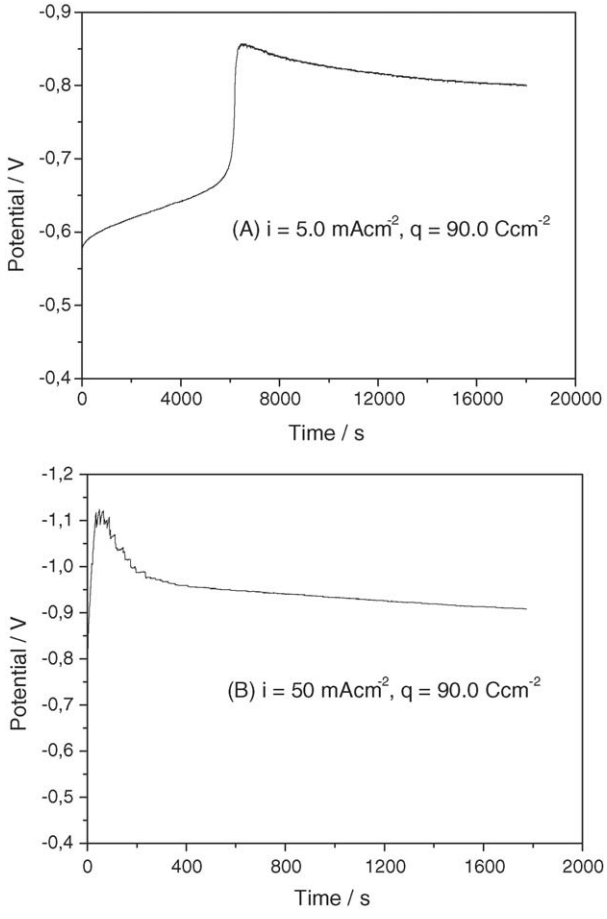

Fig. 6. Typical chronopotentiometric plot for nickel electrodeposition from leaching solution, without stirring: (A) $i = 5.0$ mA cm^{-2} and (B) $i = 50$ mA cm^{-2}, $q_{applied} = 90.0$ C cm^{-2}, 298 K.

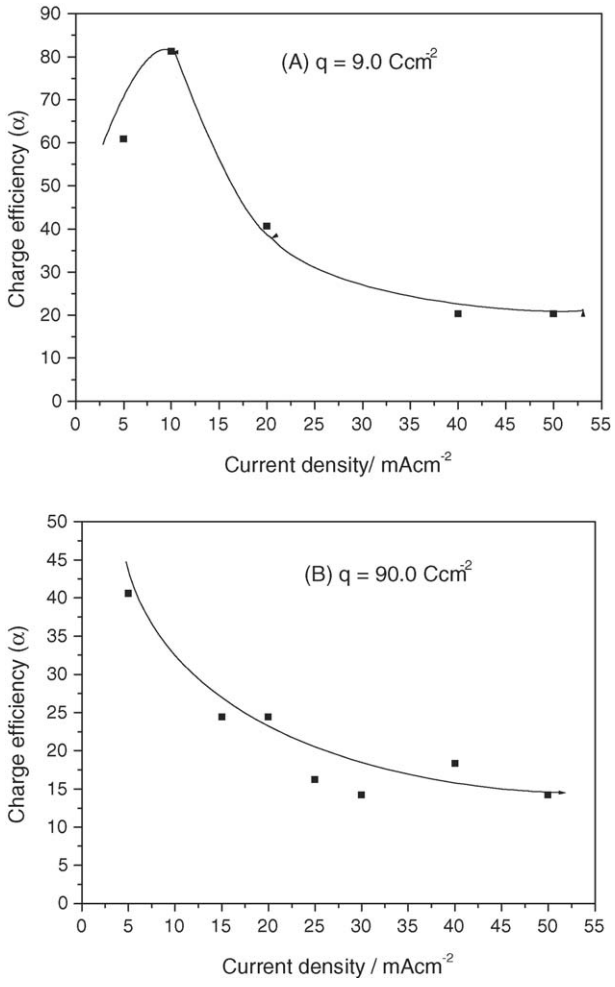

Fig. 7. Charge efficiency vs. current density for nickel electrodepositiom from leaching solution, without stirring, 298 K: (A) 9.0 C cm^{-2} and (B) 90.0 C cm^{-2}.

The current density decreased with the increase in electrode porosity. As a result, the potential led to low cathodic values with increasing electrodeposition time.

As shown in Fig. 7, the charge efficiency is higher at low current densities. In this case, the chronopotentiometric plots present the first plateau potential or little potential change during electrodeposition. This behavior corresponds to current densities between 5.0 mA cm^{-2} and 10.0 mA cm^{-2} for charge densities of 9.0 C cm^{-2} and 5.0 mA cm^{-2} for charge densities of 90.0 C cm^{-2}. It also can be seen that electrodeposition efficiency decreased with the increase in charge density. The increase in the evolution of hydrogen on metallic nickel reduced charge efficiency.

The reaction kinetics can be controlled on the electrode surface by activation and inside the pores by mass transport. There is a dual control for charge density equal to 9.0 C cm^{-2}, as shown in Fig. 8A. The relation between the potential and the current density follows the Tafel equation when it is controlled by activation, as shown in Fig. 8B for charge density equal to 90.0 C cm^{-2}. Therefore, for porous electrodes, the control of the reaction kinetics changes with charge density.

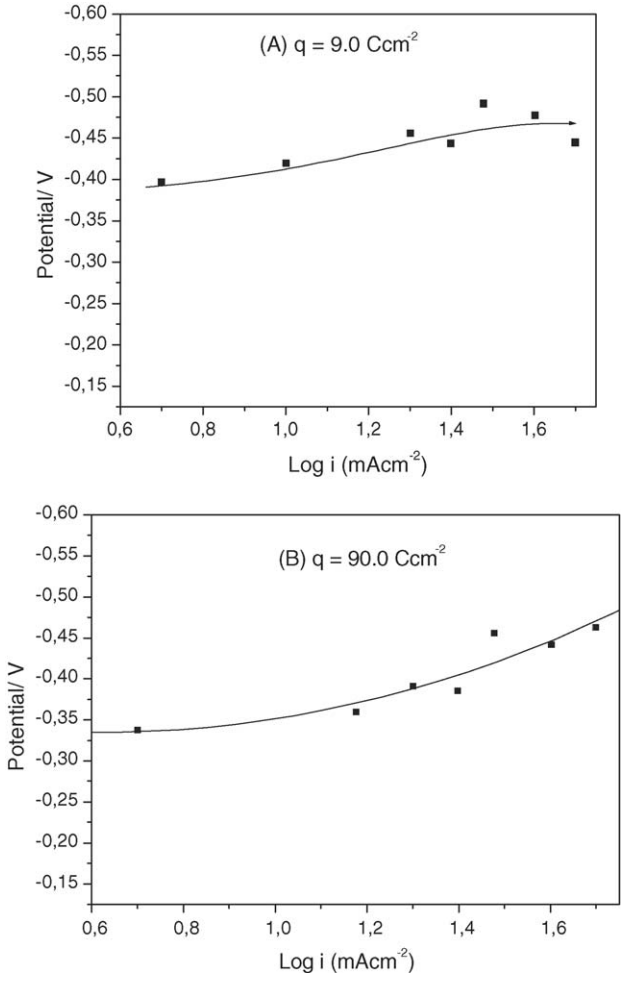

Fig. 8. Potential in function of the current density for nickel electrodeposition in acidic solution: (A) $q = 9.0\,C\,cm^{-2}$ and (B) $q = 90.0\,C\,cm^{-2}$, without stirring, 298 K.

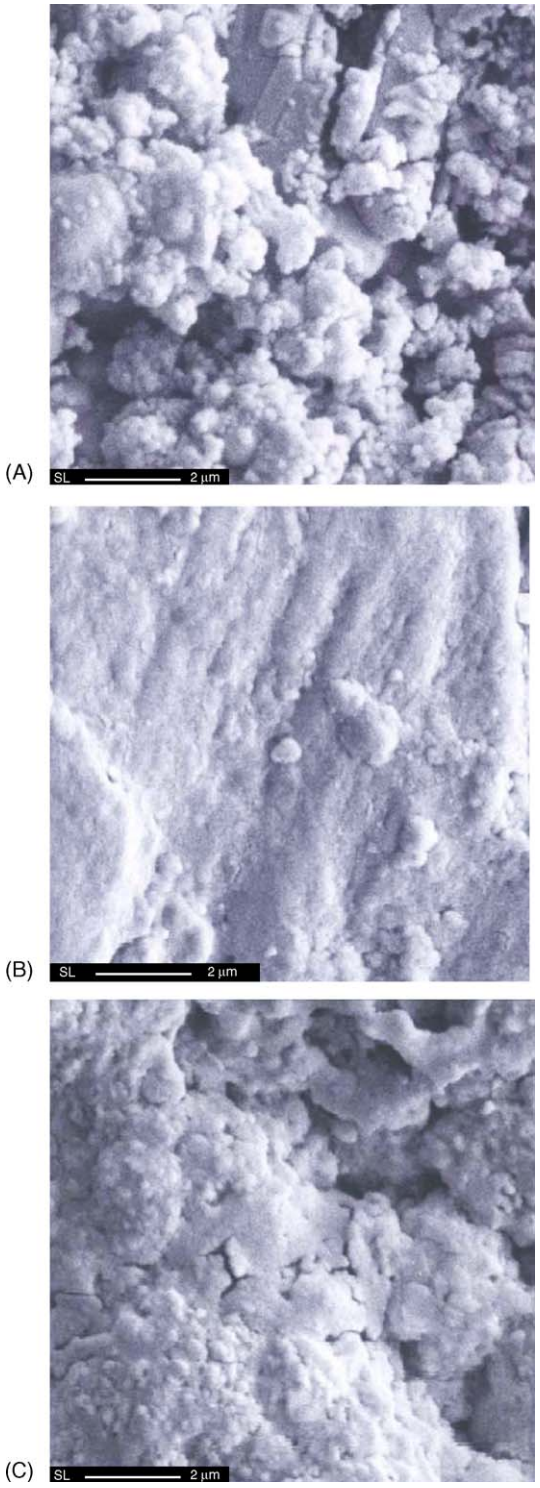

Fig. 9. Typical scanning electron microscopy for nickel electrodeposit: (A) $i = 5.0\,mA\,cm^{-2}$ and $q = 9.0\,C\,cm^{-2}$, (B) $i = 5.0\,mA\,cm^{-2}$ and $q = 90.0\,C\,cm^{-2}$, and (C) $i = 50.0\,mA\,cm^{-2}$ and $q = 90.0\,C\,cm^{-2}$.

Charge density affects not only the reaction kinetics but also deposit morphology, as shown in Fig. 9. For current densities with higher charge efficiency ($i = 5.0\,mA\,cm^{-2}$), a decrease in microporosity was observed with increase in charge density. For the same charge density, microporosity increased as the current density increased.

4. Conclusions

The investigation of the recycling process of nickel from spent Ni–Cd batteries first involved the characterization of exhausted battery electrodes. A partially discharged positive electrode contains mostly phase β-$Ni(OH)_2$/β-NiOOH and β-CoOOH. With the help of SEM, it was possible to verify a reduction of the battery useful life due to the formation of cracks on the electrodes. The appearance of these cracks results from molar volume variation in the charge–discharge cycles. With EDX, the presence of additives was verified whose function is to increase the electrode capacity, and also the presence of sulfur was found presumably from the electrolyte. The chemical precipitation for recycling of nickel as a precursor material was carried out at two different temperatures. It was observed through X-ray diffraction that the α-$Ni(OH)_2$ phase stabilized with synthesis at 279 K. With the increase in synthesis temperature, the α-$Ni(OH)_2$ phase aged and became β-$Ni(OH)_2$.

Nickel also was recycled using a galvanostatic technique with different charge densities. The reduction of ionic nickel is the principal reaction at the first plateau potential in the chronopotentiometric plot. With increase in electrodeposition time, the potential became more and more cathodic and stabilized at a second plateau potential. At this second plateau potential, the evolution of hydrogen on the nickel electrode is the principal reaction. Charge efficiency is higher for lower current densities. In this case, the chronopotentiometric plots showed the first plateau potential with little potential change during electrodeposition. Electrodeposition efficiency decreased with the increase in charge density and a second plateau potential was quickly reached. The increase in the evolution of hydrogen on metallic nickel reduced charge efficiency. On the other hand, a decrease in microporosity is observed with the increase in charge density. For the same charge density, microporosity increased with the increase in current density.

References

[1] C.J. Rydh, M. Karlström, Resour. Conserv. Recycl. 34 (2002) 289.
[2] C.J. Rydh, B. Sväd, Sci. Total Environ. 302 (2003) 167.
[3] T. Osawa, E. Kobayashi, Y. Okuro, Y. Suwazono, T. Kido, K. Nogawa, Environ. Res. Sect. A86 (2001) 51.
[4] J. McBreen, R.E. White, J.O'M. Bockris, in: B.E. Conway (Ed.), Modern Aspects of Electrochemistry, vol. 21, Plenum Press, New York, 1990.
[5] P. Oliva, J. Leonard, J.F. Laurert, C. Delmas, J.J. Braconnier, M. Figlarz, F. Fievet, A. Guibert, J. Power Sources 8 (1982) 229.
[6] R.S. McEwen, J. Phys. Chem. 12 (1971) 1782.
[7] D. Tuomi, J. Electrochem. Soc. 112 (1965) 1.
[8] M.B.J.G. Freitas, J. Power Sources 93 (2001) 163.
[9] R. Acharya, T. Subbaiah, S. Anand, R.P. Das, Mater. Lett. 57 (2003) 3089.
[10] M.P. Waalkes, J. Inorg. Biochem. 79 (2000) 241.
[11] Conselho Nacional do Meio Ambiente (CONAMA), Resolution no. 257, June 30, 1999, Diário Oficial da União (DOU) July 22, 1999.
[12] A.M. Bernardes, D.C. Espinosa, J.A.S. Tenório, J. Power Sources 130 (2004) 291.
[13] M.B.J.G. Freitas, M.K. Pietre, J. Power Sources 128 (2004) 343.
[14] M.B.J.G. Freitas, S.F. Rosalém, Power Sources 139 (2005) 366.
[15] Joint Committee on Power Diffraction Standars (JCPDS), Card No. 14-0117.
[16] Joint Committee on Power Diffraction Standars (JCPDS), Card No. 30-0443.
[17] Joint Committee on Power Diffraction Standars (JCPDS), Card No. 22-0444.
[18] Joint Committee on Power Diffraction Standars (JCPDS), Card No. 02-1094.